Timing and Setting of Gold Mineralization in the Maljavr Oc-Currence, NE Part of the Fennoscandian Shield

Arkadii A. Kalinin *, Nickolay M. Kudryashov , Yevgeny E. Savchenko

Posted Date: 26 March 2024

doi: 10.20944/preprints202403.1492.v1

Keywords: Archean conglomerate; greenstone belt; alteration; gold; bismuth; ehrigite; U-Pb age; zircon.

 doi:10.20944/preprints202403.1492.v1

Article

Timing and Setting of Gold Mineralization in the Maljavr Occurrence, NE Part of the Fennoscandian Shield

Arkadiy Kalinin *, Nickolay Kudryashov and Yevgeniy Savchenko

Geological Institute, Kola Science Center, Russian Academy of Science, 184200 Apatity, Russia; n.kudryashov@ksc.ru (N.K.); ye.savchenko@ksc.ru (Y.S.)

* Correspondence: a.kalinin@ksc.ru; Tel.: +7-921-663-68-36

Abstract: Gold occurrence Maljavr, located in amphibolite metamorphosed rocks in the Uragubsky greenstone belt, is the first gold prospect connected with conglomerates of Archean age, found in the Fennoscandian Shield. Gold mineralization is controlled by a series of lenses of altered rocks in biotite gneiss-metaconglomerate. The age of zircon from biotite gneiss in the zone of alteration is 2665±22 Ma, this is considered as the time of alteration processes. Biotite gneiss and altered rocks were later intruded by tourmaline granite pegmatite at 2508±7Ga, the pegmatite caused recrystallization of sulfide minerals in the altered rocks. Visible gold in association with bismuth minerals native bismuth, ehrigite (the second finding in the world), maldonite, bismuthinite, joseite-B, hedleyite was found exceptionally in polymineral inclusions in recrystallized arsenopyrite and löllingite. The age of pegmatite 2508±7Ma we regard as the time of formation of gold-bismuth mineralization. Geological position of the Maljavr occurrence, the linkage of gold mineralization with pegmatite, geochemical association Au-As-Se-Te-Bi in the mineralized rocks – all these characteristics correspond to intrusion-related gold deposits. Biotite gneiss-metaconglomerate, hosting the mineralized altered rocks, was the probable primary source of arsenic and gold for mineralization.

Keywords: Archean conglomerate; greenstone belt; alteration; gold; bismuth; ehrigite; U-Pb age; zircon

1. Introduction

Modified paleoplacers in the Precambrian conglomerates are the most important genetic type of gold deposits: half of gold ever mined on the Earth was mined from Witwatersrand Mesoarchean conglomerate basin in South Africa [1]. Conglomerates with gold are known in other Precambrian shields in the world as well – for example, Tarkwa in Ghana (Western Africa) [2], Jacobina in Brazil (South America) [3], in Pilbara craton (Australia) [4], in craton Singhbhum (India) [5], Pardo in Canada [6,7]. High gold grades are connected mainly with alluvial placers along river paleovalleys, but sea beach paleoplacers are also known (in Australia – [4]. In the Fennoscandian shield, conglomerates with gold were found in the Lehtinskaya and Onezhskaya structures in Karelia, these gold occurrences are considered as modified Paleoproterozoic gold paleoplacers in fluvio-deltaic fans [8].

Gold-bearing conglomerates are either monomictic with quartz pebbles or polymictic with pebbles of different composition, up to ultramafic pebbles. Gold concentrates mainly in the conglomerate cement, not in the pebbles. The cement may be clayey, sandy, up to coarse-grained sands. Paleoplacers (and gold as a mineral) were modified during late regional metamorphic and hydrothermal-metasomatic events. If these modifying events were intensive, then gold deposits and occurrences display features of orogenic or intrusion-related deposits, where paleoplacers played a role of interim gold concentrators. Gold occurrence Maljavr, located in amphibolite metamorphosed rocks in the Uragubsky greenstone belt (north-eastern part of the Fennoscandian Shield), is an

 doi:10.20944/preprints202403.1492.v1

occurrence of this type. It is the first gold occurrence connected with conglomerates of Archean age, found in the Fennoscandian Shield.

2. Materials and Methods

Gold mineralization was studied in the specimens and samples (1.5 – 10 kg), collected by the authors in the outcrops and trenches in 2022-2023. Investigations of wallrock alteration, metasomatic zoning, and determination of pre-ore, ore-related, and post-ore mineral assemblages in altered rocks were based on the study of rocks in the outcrops, on examination of mineral relations in thin and polished sections, as well as on the results of assaying the primary and altered rocks. The samples were assayed for major (rock-forming) elements in the chemical laboratory of the Geological Institute, Kola Science Centre of Russian Academy of Sciences, Apatity, Russia, with flame atomic absorption spectrometry (FAAS). Data on trace elements, which determined the geochemical characteristics of the rocks, were obtained by ICP-MS in the Institute of Geology and Geochemistry of the Ural Branch of the Russian Academy of Sciences, Ekaterinburg,

Mineral composition of the ores was studied in thin and polished sections with reflected light microscope Axioplan 2 Imaging (Karl Zeiss, Jena, Germany) and with the electron microscope Zeiss Evo-25 (Carl Zeiss, Jena, Germany), equipped with the energy-dispersive system (EDS) AZtec UltimMax-100 (Oxford Instruments) in the Geological Institute of the Kola Science Center. All mineral phases were identified and photographed in the regime of back-scattered electron image (BSE). Chemical composition of mineral phases was defined with EDS AZtec UltimMax-100 (Oxford Instruments), operating at accelerating voltage 20 kV, beam current 2 nA, spectrum accumulation time 100 s. The following analytical lines and standards were used for silicates and oxides: FKα (fluorapatite), SiKα and CaKα (wollastonite), ClKα (atacamite), FeKα (hematite), LaLα (LaSe), CeLα (CeS), NdLα (LiNd(MoO4)2), TiKα and NaKα (lorenzenite), MnKα ($MnCO_3$), SKα, and SrLα, MgKα, AlKα, KKα, NiKα (metal); analytical lines (standards) for sulfides and metals were PbMα and TeLα (PbTe, in some cases HgTe for TeLα) , BiMα and SeLα (Bi2Se3), AsKα (InAs), AgLα (metal), AuMα (metal), FeKα и SKα (pyrite) (in some cases metal for FeKα), NiKα (metal), CoKα, (metal), ZnKα (metal or sphalerite), BrKα (KBr), CdLα (metal or CdSe).

Microprobe analysis (MS-46, CAMECA, Gennevilliers Cedex, France), accelerating voltage 22 kV, beam current 30–40 nA, standards (analytical lines; detection limit, wt.%): $Fe_{10}S_{11}$ (FeKα; 0.01 and SKα; 0.05), Bi_2Se_3 (BiMα; 0.1 and SeKα; 0.05), LiNd(MoO4)2 (MoLα; 0.1), PbS (PbMα; 0.1), pure metals Co (CoKα; 0.01), Ni (NiKα; 0.01), Cu (CuKα; 0.01), Pd (PdLα; 0.05), Ag (AgLα; 0.05), Te (TeLα; 0.05), Re (ReLα; 0.05), Au (AuLα; 0.05), was performed for grains larger than 20 μm (analyst Ye. Savchenko). Beam size was 2–10 nm, depending on stability of the matter under the beam current. Measurement time was 10s for major elements, 20s for minor elements, and 10s for background measurements. The results of 4–5 measurements for each element were averaged.

Zircon U–Pb dating was undertaken at the Geological Institute of the Kola Science Center. Prior to analysis, zircons were extracted using standard magnetic and heavy liquid separation, with surface contamination removed using alcohol, acetone, and 1 M HNO_3.

The zircon dissolution and chemical recovery of Pb and U was performed using the technique described in [9], with U and Pb concentrations determined by isotope dilution employing a Finnigan MAT-262 (RPQ) mass spectrometer and a mixed ^{208}Pb + ^{235}U tracer, with silica gel used as an ion emitter. Blank levels had maximum values of 100 ng Pb and 10–50 ng U, and all isotope ratios were corrected for mass fractionation by analysis of the SRM-981 and SRM-982 standards (0.12 ± 0.44%). The uncertainties on the resulting U–Pb ratios are 0.5%. The raw experimental data were processed using PbDAT and ISOPLOT [10, 11], with age values calculated using conventional U decay constant values [12] and common Pb corrections following [13]. All uncertainties are reported at a 2σ confidence level.

 doi:10.20944/preprints202403.1492.v1

3. Results

3.1. Geological Overview of the Study Area

The Maljavr gold occurrence is located within the Uragubsky greenstone belt, which traces the boundary between the Murmansk craton and the Kola-Norwegian province (or simply Kola province) of the Fennoscandian Shield (Figure 1, inset).

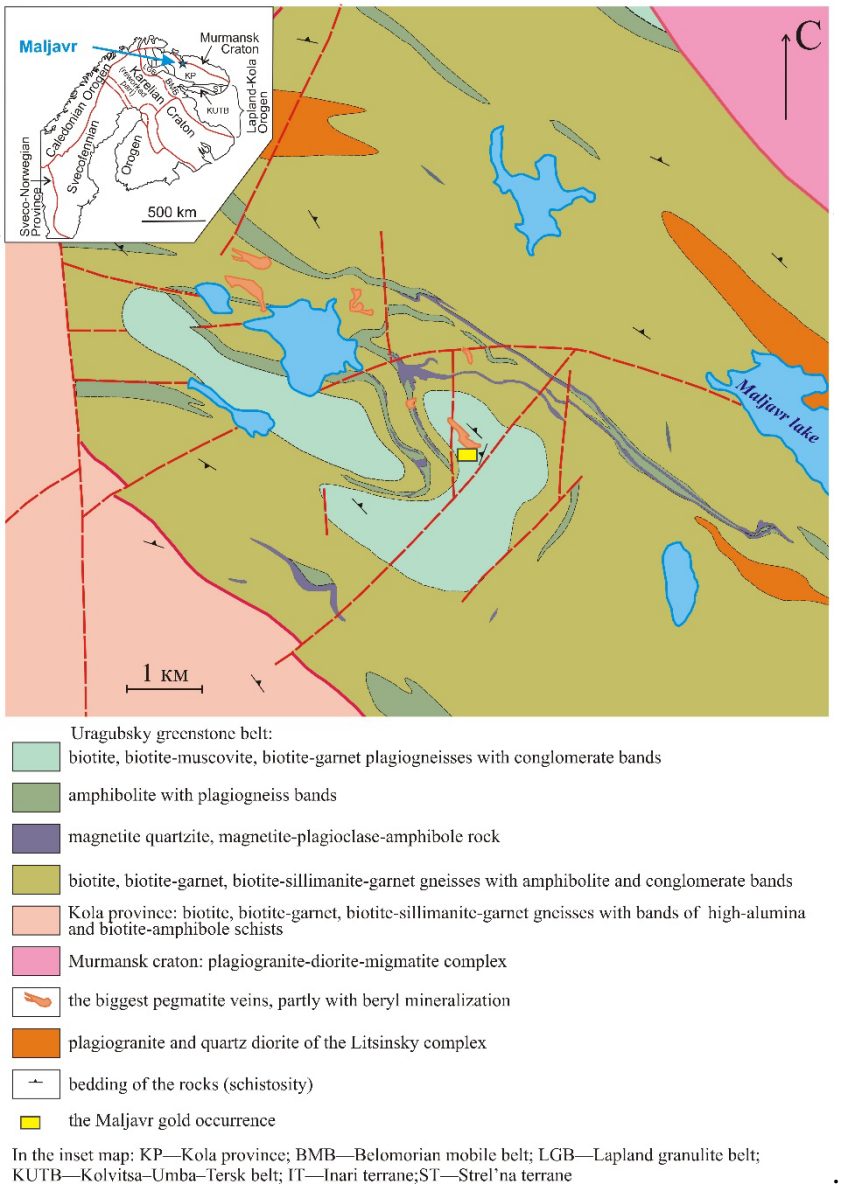

Figure 1. Schematic geological map of the Maljavr gold occurrence area, designed using data from [14], and position of the Maljavr occurrence in the tectonic map of the Fennoscandian Shield (inset).

The Uragubsky belt is a north-western prolongation of the larger and more extensive Kolmozero-Voron'ya greenstone belt with big rare metal Li-Cs-Ta pegmatite deposits and numerous gold occurrences. Geological section of the Uragubsky belt is generally reduced relative to the Kolmozero-Voron'ya, but comprises a basal terrigenous sequence. Metasedimentary rocks prevail in the lower part, and the share of metavolcanics from ultramafic to acidic composition increases in the middle and upper parts of the section of the Uragubsky belt [15].

The lower terrigenous sequence is composed mainly of fine and medium grained biotite and two-mica gneisses and cataclastic pebble and boulder–pebble rocks. The middle sequence is composed of mafic-ultramafic volcanic, it also contains tuff horizons, fine-grained biotite and biotite–

 doi:10.20944/preprints202403.1492.v1

amphibole gneiss horizons and lenses, layers of magnetite quartzite and magnetite-amphibole rocks (Figure 1). The upper sedimentary-volcanic sequence consists predominantly of biotite, biotite–garnet, biotite–staurolite–sillimanite, biotite–sillimanite–garnet gneisses with subordinate thin foliated amphibolite bodies. Chemical composition of the gneisses corresponds to dacite and rhyolite; paragneisses are subordinate. The U-Pb SHRIMP II age of zircon from gneiss-metadacite is 2838 ± 23Ma, this age is considered as the age of volcanism [16,17].

The volcanic-sedimentary rocks were amphibolite metamorphosed at a temperature of 600–620°C, under a pressure of 4 kbar [18]. The U-Pb age of metamorphism was reported 2786 ± 31, 2774 ± 12 Ma (SHRIMP-II, zircons of metamorphic genesis) [16], 2763 ± 8 Ma [15].

The volcanic-sedimentary sequences are cut by intrusions of plagiomicrocline granite (2696 ± 9 Ma), aplite veins (2697 ± 10 Ma) [19], and tourmaline granite pegmatite veins.

Pebble conglomerates were mapped in the lower part of the basal terrigenous sequence, at the southern contact of the belt with migmatized gneisses and plagiogranites of the Kola province [15,20,21]. Thickness of the conglomerate layer is 2-5m, sometimes up to 10 m. Pebble content does not exceed 30–35% of the total volume of the conglomerate, the dimensions of pebbles vary predominantly from 3×5 to 5×10 cm. Fine grained greywacke (biotite and muscovite-biotite gneiss) makes the conglomerate cement.

Layers and lenses of pebble conglomerate and gritstone were also observed throughout the entire biotite gneiss sequence. Every conglomerate layer is an alternation of of conglomerate, gritstone, and sandstone (Figure 2) with thickness of strata 10-20 cm. The rocks preserved obvious signatures of their terrigenous origin such as graded rhythmical bedding and psephytic–psammitic structures. The clasts consist predominantly of plagiogranite (up to diorite) and quartz; pebbles and gravel are cemented by biotite- or biotite-muscovite gneiss-metagraywacke. Plagiogranite in the pebbles contains oligoclase, partly sericitizated, quartz, and minor biotite and tourmaline. Gneiss in the cement consists of quartz, plagioclase (labradorite), biotite, ±muscovite; accessory minerals are apatite, zircon, chlorite, tourmaline, allanite. The gneiss in the cement is similar to the biotite paragneiss in the lower sequence of the volcanic-sedimentary section.

Figure 2. Graded rhythmical bedding in conglomerate in an outcrop (left) and in a block.

 doi:10.20944/preprints202403.1492.v1

3.2. The Maljavr Occurrence: Geological Structure, Alteration, Ore Minerals

Gold occurrence Maljavr is located at the SW flank of the belt, where biotite gneiss of the lower sequence forms an anticline fold with the upper bend dipping SE (Figure 1). Biotite gneiss (metamorphosed sandstone, gritstone, and conglomerate) is cut by a tourmaline granite pegmatite vein of sub-meridional strike, about 40 m thick (Figure 3). Rock forming minerals in pegmatite are quartz, plagioclase (albite-oligoclase), microcline, muscovite and tourmaline, minor minerals are biotite, apatite, zircon.

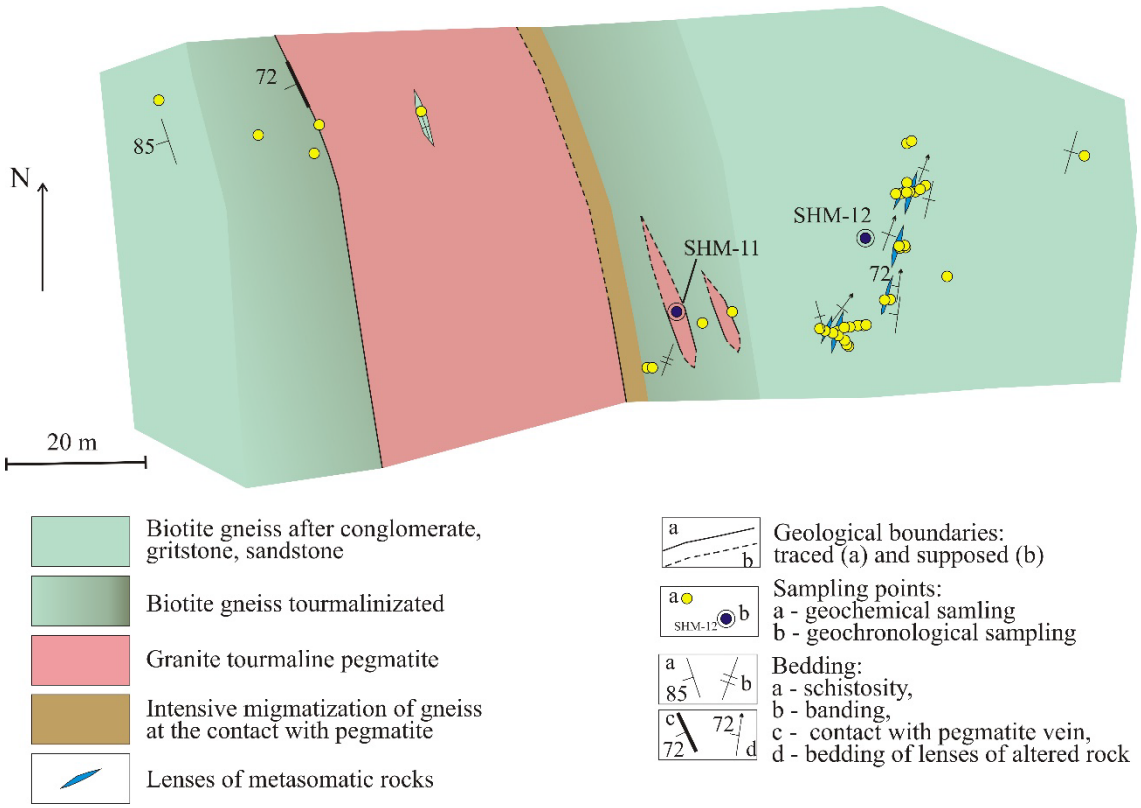

Figure 3. Schematic geological map of the Maljavr gold occurrence.

The western contact of the vein is sharp linear, but the eastern contact is transitional, through a zone of migmatization and foliation ~10 m wide. In the zone of foliation, pebbles are deformed together with the cement (Figure 4,A). The biotite gneiss is intensely tourmalinizated at both sides of the pegmatite vein (Figure 3). Deformation and tourmalinization intensity in the biotite gneiss decreases within ~20m distance from the pegmatite contact.

Smaller lenses of pegmatite were found up to 50 m away from the main pegmatite vein and zone of migmatization. The biggest lenses are up to 20 m long, smaller lenses are less than 20-30 cm. The pegmatite lenses cut biotite gneiss, including the pebbles in metaconglomerate (Figure 4,C).

A series of lenses of altered rocks makes a zone ~10 m thick, which strikes NNE 10-15° conformably to shistosity in the biotite gneiss (Figure 3). The zone of alteration was traced for 50 m in the outcrop, farther it is covered by soil.

Lenses of metasomatic rocks reach the length of 10 m and 1 m thickness (Figure 3). The lenses clearly exhibit three alteration envelopes (Figure 5). Hornblende and hedenbergite are the principal rock-forming minerals in the outer zone, where minor minerals are epidote, quartz, and garnet. Biotite, garnet, and quartz make the intermediate biotite-garnet envelope. The central parts of the lenses consist of garnet and quartz or garnet-only (garnetite) (Figure 3,5). The outer hornblende-hedenbergite envelope is reduced in some lenses (Figure 5).

Metasomatic rocks are massive, medium- to coarse-grained: garnet grains reach 1 cm, other minerals are 1-3 mm big. Biotite flakes and needle crystals of amphibole and pyroxene are differently

 doi:10.20944/preprints202403.1492.v1

oriented. Quartz veinlets penetrate all zones of metasomatic rocks, the veinlets are oriented along the strike of the lenses (Figure 5).

Figure 4. Photographs of outcrops in the Maljavr occurrence. A – foliation in the biotite gneiss-metaconglomerate; B – migmatization at the contact of biotite gneiss with pegmatite; C and D – small pegmatite lenses, cutting schistosity in metaconglomerate.

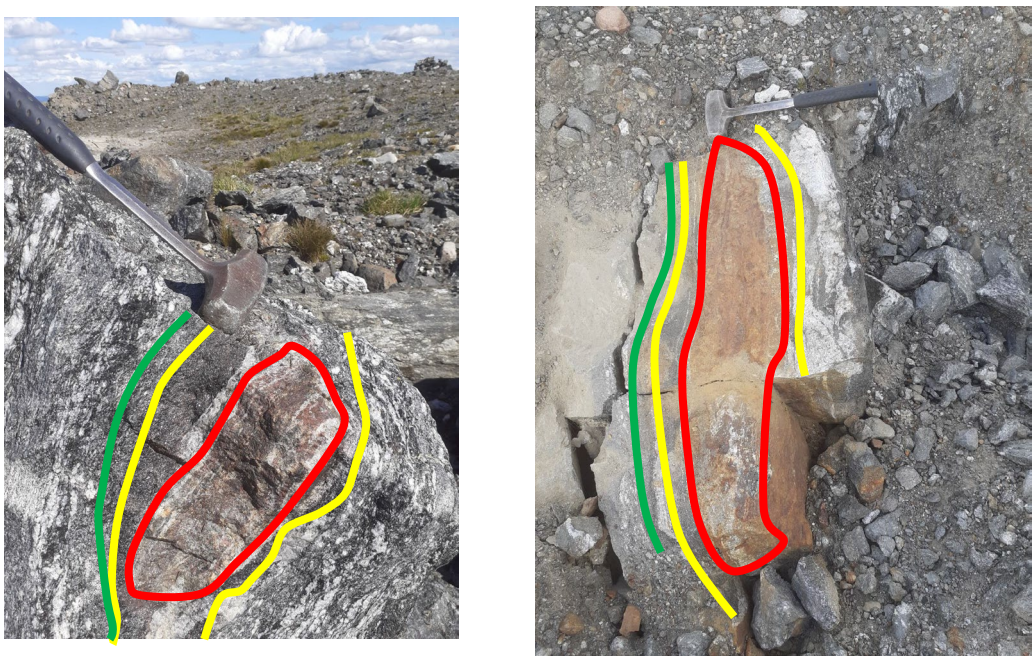

Figure 5. Lenses of altered rocks in the metaconglomerate: red, yellow and green – boundaries of garnet-quartz, biotite-garnet and hornblende-hedenbergite metasomatic rocks, correspondingly.

The spidergrams (Figure 6) illustrate change chemical composition of the rocks during alteration processes. The diagrams exhibit general loss of SiO_2 and Na_2O, and gain of FeO in the altered rocks. Al_2O_3, CaO, MgO, K_2O were re-deposited during alteration and formed metasomatic zoning.

 doi:10.20944/preprints202403.1492.v1

Hornblende-hedenbergite rock has high CaO, low Al_2O_3, Na_2O, and K_2O. Biotite-garnet rock contains high Al_2O_3, MgO, and K_2O, but low CaO. Garnet-quartz rock in the central part of the lenses has high FeO, and lower content of other general elements (Table S1).

Change of mineral composition of the rocks during alteration processes is chiefly limited to decomposition of plagioclase in the biotite gneiss, recrystallization of biotite and quartz and formation of garnet, amphiboles, and pyroxene. Sodium, released during plagioclase decomposition, was taken away from the altered rocks. Calcium was re-deposited in the outer hornblende-hedenbergite envelope, where it formed Ca-rich hornblende, hedenbergite, and high-Ca almandine. The residual alumina from the decomposed plagioclase together with iron, which was added to the system, formed garnet (almandine) in biotite-garnet and garnet-quartz rocks. Potassium, concentrated in the primary biotite in gneiss, was re-deposited mainly in the garnet-biotite rock.

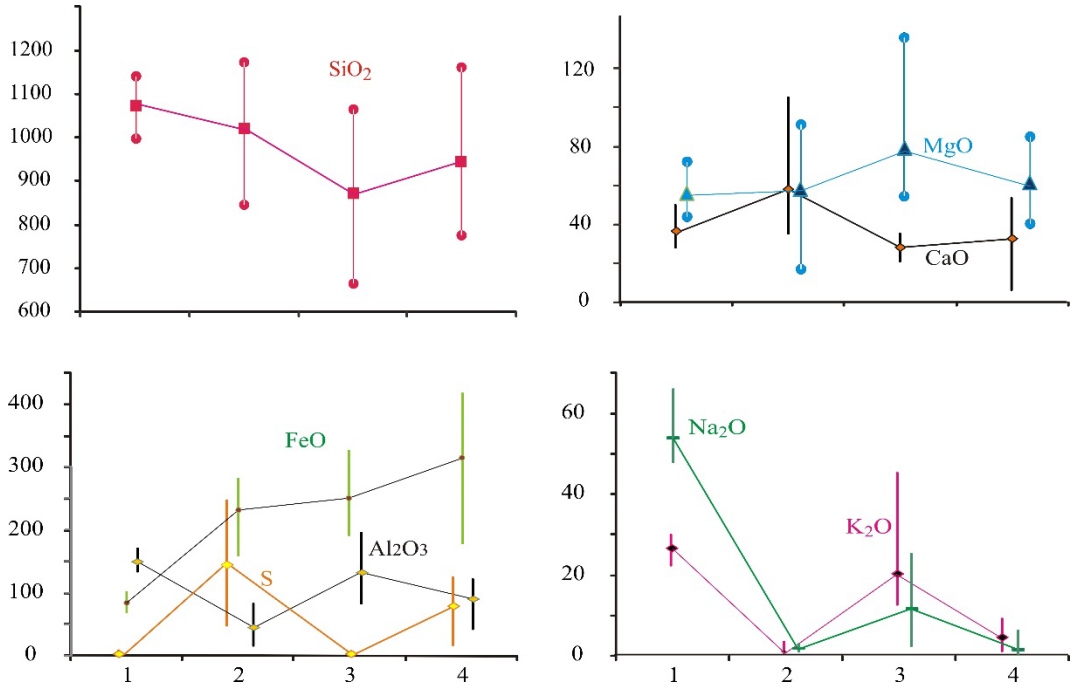

Figure 6. Variation of the main components content in altered rocks: maximum, minimum and mean values, in molar quantities. Rocks: 1 – unaltered biotite plagiogneiss (8 samples), 2-4 – altered rocks: 2 – hornblende-hedenbergite (11), 3 – garnet-biotite (5), 4 – garnet-quartz and garnet-only (10 samples) (see Table A1 for assay results).

GER diagrams [22] (Figure 7) illustrate change of both mineral and chemical composition during alteration and formation of metasomatic zoning in terms of element ratios: loss of sodium due to decomposition of plagioclase (Figure 7, A,B), redistribution of potassium, connected with recrystallization of biotite (Figure 7, A,B), addition of Fe and redistribution of Ca and Al, which lead to formation of Ca-rich almandine, hornblende, and hedenbergite (Figure 7, C,D).

 doi:10.20944/preprints202403.1492.v1

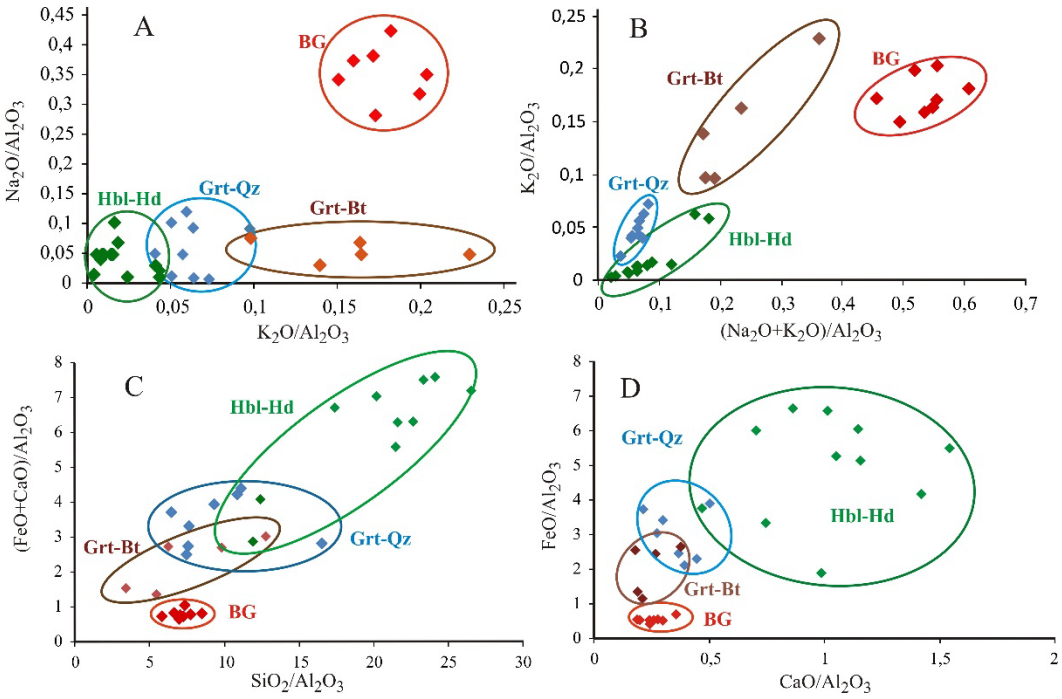

Figure 7. GER diagrams [22] for altered rocks of the Maljavr occurrence. BG - unaltered biotite gneiss. Altered rocks: Gr-Qz – garnet-quartz rock, Grt-Bt – garnet-biotite rock, Hbl-Hd – hornblende-hedenbergite rock. Here and below all mineral symbols are given according to IMA recommendations [23].

All Fe-Mg silicates in the altered rocks are Fe-rich (Table S2): pyroxene is hedenbergite, amphiboles are ferro-hornblende and grunerite, chlorite is chamosite, and mica is Fe-biotite. Garnet is almandine, but almandine is Ca-rich in the hornblende-hedenbergite rock: mole proportion of grossular is 14-28% (Table S2), increasing in the outer parts of the zoned almandine crystals.

Altered rocks, if compared with the unaltered biotite gneiss, display loss of Rb, Cs, Sr, Ba, Zr, Nb, LREE, U, Pb, and gain of As, Ag, Te, Se, Bi, Cu (Table S3, Figure 8). It is important to note high As in the unaltered biotite gneiss, arsenic is 3–15 times higher than the average for the upper continental crust [24]. Concentration of As, Te, Se, and Bi in gold-mineralized rocks is by 1-2 orders of magnitude more than in non-mineralized metasomatic rocks (Table S3).

 doi:10.20944/preprints202403.1492.v1

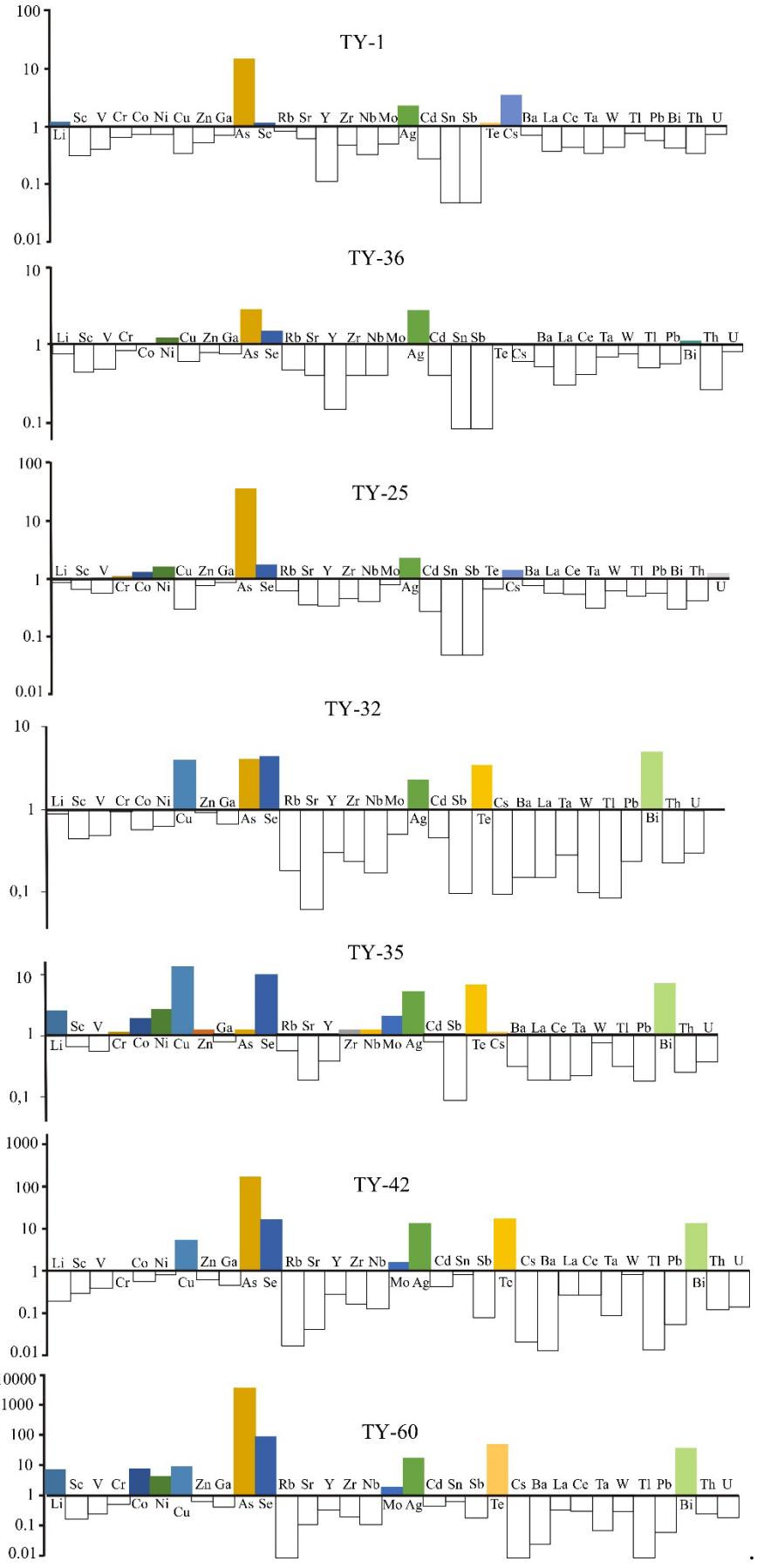

Figure 8. Geochemical spectra of unaltered biotite gneiss-metaconglomerate (TY-1 и TY-36), slightly altered biotite gneiss at the contact with a lens of altered rock (TY-25), not gold-mineralized altered

 doi:10.20944/preprints202403.1492.v1

rocks (TY-32, TY-35), and gold-mineralized altered rocks (TY-42, TY-60), normalized by the average for the upper continental crust [24].

Gold content in the unaltered biotite gneiss is close to the average in the continental crust, and increases in altered rocks. Channel sampling across one of the lenses of altered rocks gave 1.78 g/t for 0.8 m [14], but gold content in hand samples reaches 30 g/t.

Unaltered biotite gneiss (metaconglomerate, metagritstone, metasandstone) contains disseminated sulfide mineralization <1 vol.%; sulfide minerals are pyrrhotite (prevails), arsenopyrite, rarely chalcopyrite, and late pyrite; oxide minerals are ilmenite and rare magnetite. No sulfide mineralization was found in the migmatizated rocks at the contact of biotite gneiss with pegmatite.

Sulfide content increases significantly in the lenses of altered rocks, but distribution of sulfide mineralization is very uneven, varying from 1 to 25 vol.%. Sulfide-rich rocks were found in different envelopes of the lenses, texture of mineralization is disseminated, veinlet-disseminated, or nested. Mineral composition is not complicated: the main minerals are pyrrhotite and arsenopyrite, minor sulfides are chalcopyrite, löllingite, troilite, pentlandite. Oxide minerals are ilmenite and magnetite (more rare, but up to 10% in some samples).

Two generations of arsenopyrite were detected in the metasomatic rocks, the generations differ in grain form and size (Figure 9), and in chemical composition (Table 1). The early arsenopyrite-1 occurs as disseminated grains up to 0.2 mm. It contains high Co and Ni, and some grains are clearly zoned (Figure 9) with As-, Co- and Ni-rich core (As 38.2 – 39.7 at%, Co 3.12 – 4.11 mas.%, Ni 1.62 – 2.89 mas.%) and lower As, Co and Ni in the rim (As 34.6 – 35.0 at%, Co 2.23 – 2.44, and Ni 0.38 – 0.81 mas.%) (Table 1). Late re-crystallized coarse-grained (0.5 – 3 mm in size) arsenopyrite-2 is disseminated in the altered rocks, or it forms chains of euhedral grains (Figures 9,10). Zoning in arsenopyrite-2 is complicated – zones with lower (32,7 – 33,8 at.%As) and higher (34,6-35,9 at.%As) arsenic alternate in the grains (Figure 9); Co and Ni impurities are below 0.5 mas.%.

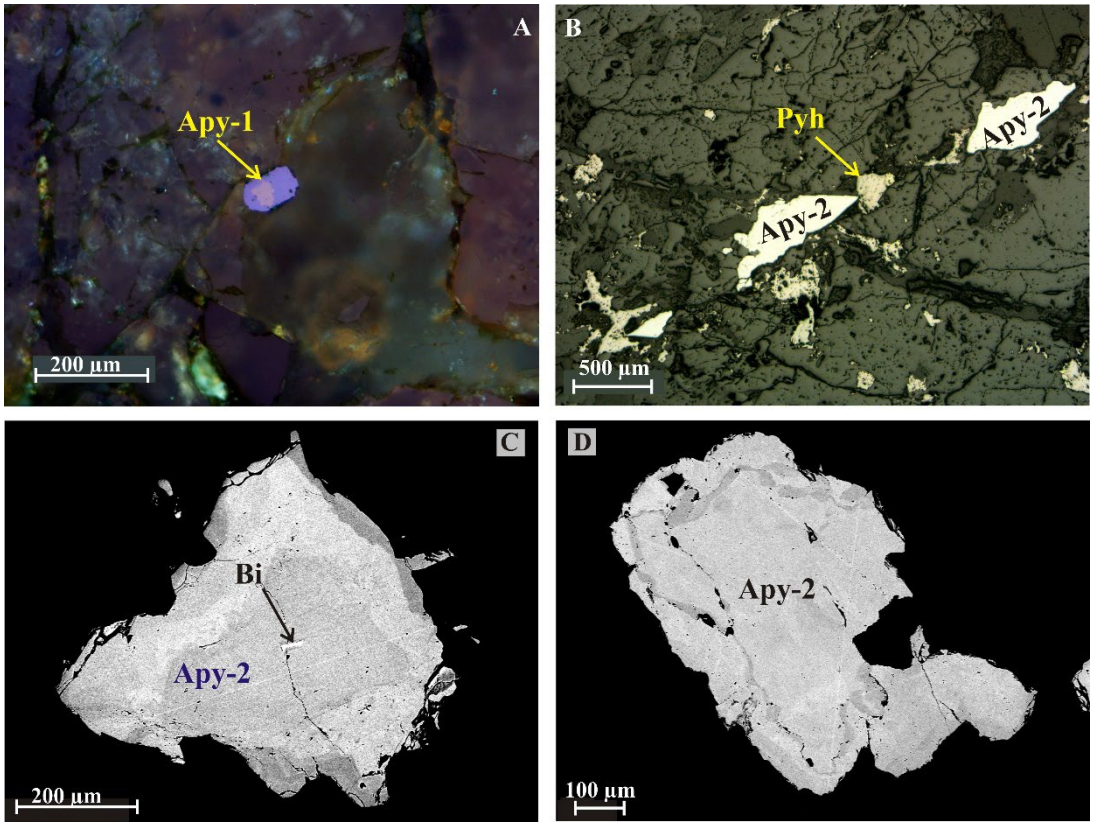

Figure 9. Arsenopyrite from the Maljavr gold occurrence. A – zoning in arsenopyrite-1, polished section photo, crossed polarized light. B – a chain of arsenopyrite-2 grains in hornblende-hedenbergite

 doi:10.20944/preprints202403.1492.v1

rock, polished section photo, plane polarized light. C and D – complicated zoning in arsenopyrite-2 – back-scattered electron (BSE) images: arsenic-rich zones are lighter than arsenic-poor. Apy – arsenopyrite, Bi – native bismuth.

Table 1. Microprobe data for arsenopyrite (Apy) and löllingite (Lo) of the Maljavr gold occurrence, mas.%.

Sample No.	ТУ-25-1	ТУ-25-1	ТУ-25-2	ТУ-25-2	ТУ-31	ТУ-31	ТУ-41	ТУ-41	ТУ-45	ТУ-45
Mineral	Apy-1-C	Apy-1-R	Apy-1-C	Apy-1-R	Apy-1-C	Apy-1-R	Apy-1-C	Apy-1-R	Apy-1-C	Apy-1-R
S	14,94	18,32	16,08	18,94	15,49	18,36	18,16	20,03	17,93	19,28
Fe	26,46	31,4	27,92	30,56	27,73	31,49	33,15	34,61	31,89	33,65
Co	3,76	2,32	3,12	2,44	4,11	2,23	0,47	0,13	1,28	0,48
Ni	2,89	0,64	2,25	0,81	1,62	0,38	0,24	bdl	0,29	0,02
As	51,83	47,69	50,57	47,45	50,93	46,8	47,86	45,47	48,52	46,38
Total	99,88	100,37	99,93	100,2	99,88	99,26	99,88	100,25	99,91	99,81
Atoms per formula unit										
S	0,805	0,946	0,852	0,965	0,831	0,957	0,94	1,014	0,927	0,986
Fe	0,819	0,931	0,850	0,894	0,854	0,942	0,985	1,006	0,946	0,987
Co	0,110	0,065	0,090	0,068	0,120	0,063	0,013	0,004	0,036	0,013
Ni	0,085	0,018	0,065	0,023	0,048	0,011	0,007	0,000	0,008	0,001
As	1,195	1,054	1,148	1,035	1,169	1,043	1,06	0,986	1,073	1,014
at% As	39,7	35,0	38,2	34,7	38,7	34,6	35,3	32,7	35,9	33,8

Table 1. (ending).

Sample No.	TY-41-1	TY-41-1	TY-41-2	TY-41-2	TY-29	TY-42	TY-42	TY-41	TY-41	TY-29	TY-42	TY-42
Mineral	Apy-2-C	Apy-2-R	Apy-2-C	Apy-2-R	Apy-2	Apy-2	Apy-2	Lo	Lo	Lo	Lo	Lo
S	18,66	19,30	17,77	19,28	17,37	18,06	18,21	1,40	1,98	1,84	1,83	2,04
Fe	33,25	34,54	33,43	34,36	33,78	33,62	33,63	27,66	28,23	28,03	25,11	26,31
Co	0,34	0,12	0,39	0,09	0,07	0,24	0,17	0,08	0,13	0,10	0,49	0,42
Ni	0,49	bdl	0,38	bdl	0,17	0,26	0,11	0,09	0,10	0,13	2,07	0,68
As	47,96	46,72	48,59	45,80	48,80	47,87	48,09	70,27	69,35	69,94	70,26	70,04
Total	100,70	100,67	100,55	99,53	100,19	100,05	100,21	99,51	99,79	100,04	99,76	99,49
Atoms per formula unit												
S	0,952	0,982	0,921	0,992	0,908	0,937	0,939	0,089	0,125	0,116	0,114	0,127
Fe	0,975	1,009	0,996	1,015	1,014	1,001	0,996	1,009	1,024	1,013	0,904	0,944
Co	0,009	0,003	0,011	0,002	0,002	0,007	0,005	0,003	0,004	0,003	0,017	0,014
Ni	0,014	0,000	0,011	0,000	0,005	0,007	0,003	0,003	0,003	0,004	0,071	0,023
As	1,048	1,018	1,079	1,008	1,092	1,063	1,061	1,911	1,875	1,884	1,886	1,873
at% As	34,9	33,8	35,7	33,4	36,1	35,2	35,3	63,4	61,8	62,4	63,0	62,8

Note: bdl=below the detection limit. Atoms per formula unit are calculated for As+S=2. Apy-1 and Apy-2 – arsenopyrite of the first and the second generations, correspondingly. C – data for the central part of the grain, R- data for the rim.

 doi:10.20944/preprints202403.1492.v1

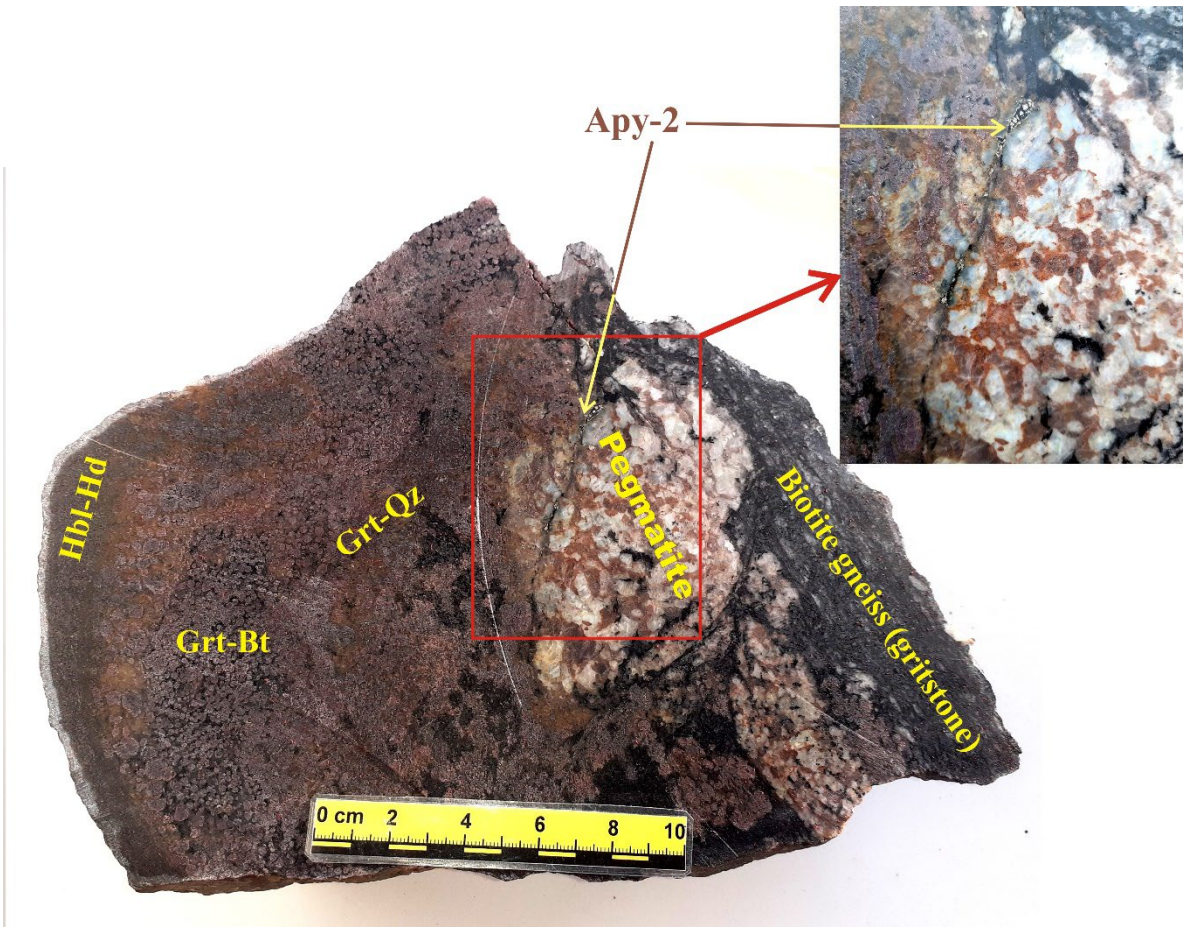

Figure 10. Pegmatite lenses, cutting biotite gneiss and metasomatic rock, a specimen photo with detail area. The arrows point at a chain of arsenopyrite-2 grains in a thin biotite veinlet between two pegmatite lenses. Apy –arsenopyrire, Bt – biotite, Grt – garnet, Hbl – hornblende, Hd – hedenbergite, Qz – quartz.

Löllingite occurs as inclusions in arsenopyrite-2 (Figure 11), rarer as separate euhedral grains up to 0.5 mm in size. Löllingite contains impurities of Ni (< 2 mas.%), Co (<0.5 mas.%), and S (< 2 mas.%) (Table 1).

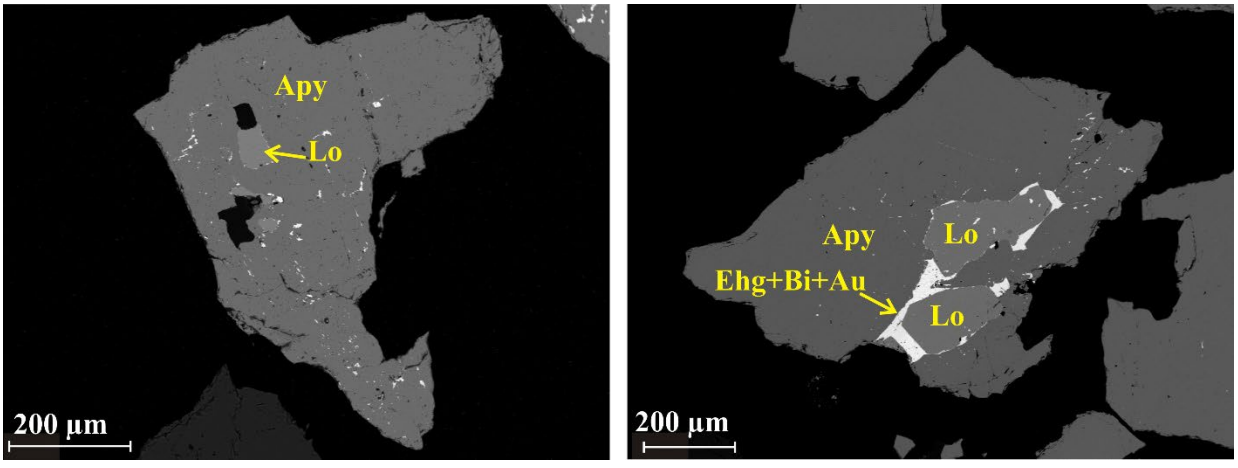

Figure 11. Inclusions of löllingite, gold, native bismuth and ehrigite in arsenopyrite-2, BSE-images. Apy – arsenopyrite, Au – native gold, Bi – native bismuth, Ehr – ehrigite, Lo – löllingite.

 doi:10.20944/preprints202403.1492.v1

Gold was found exceptionally in numerous monomineral and polymineral inclusions in arsenopyrite-2 and löllingite, together with native bismuth and bismuth telluride ehrigite Bi_8Te_3 (the second finding in the world after Good Hope gold mine [25]) (Table 2, Figures 11,12). Rarer mineral phases, found in the inclusions, are maldonite, bismuthinite, joseite-B, hedleyite, and hessite. The inclusions are of irregular angular form, up to 0.2 mm sized (Figure 12). High concentration of bismuth–ehrigite–gold inclusions is reached at the contact arsenopyrite–löllingite, or these minerals form veinlets along arsenopyrite–löllingite boundary (Figure 11).

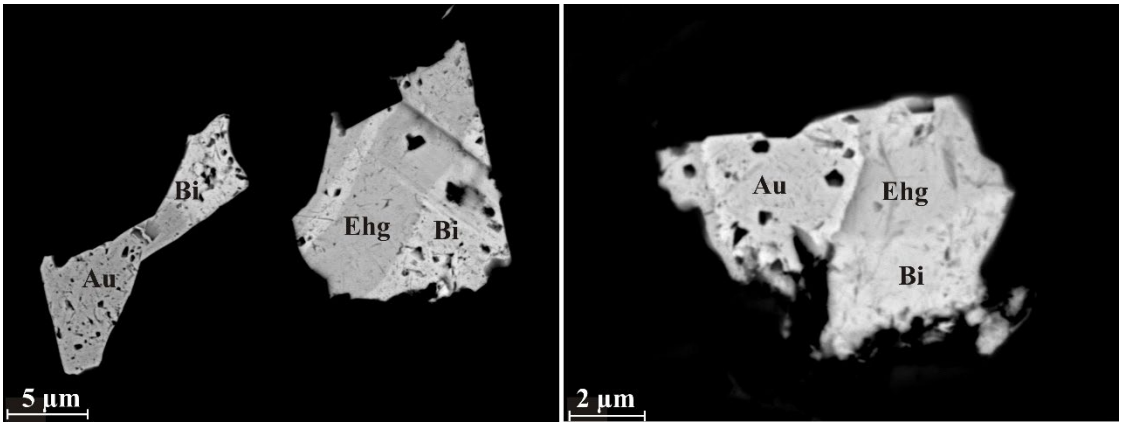

Figure 12. Polymineral inclusions of gold (Au), native bismuth (Bi) and ehrigite (Ehg) in arsenopyrite-2 (black), BSE-images. Au – native gold, Bi – native bismuth, Ehr – ehrigite.

Native gold is of high- or medium-grade, it contains from 70 to 96 mas.% Au, commonly 72 – 82 mas.%, the main impurities are Ag (4 – 30 mas.%), Fe and As (<0.2 mas.%) (Table 3). One more gold mineral in the deposit is maldonite Au_2Bi (Table 2), which occurs in the inclusions in arsenopyrite and löllingite together with gold, native bismuth, and ehrigite (Figure 13).

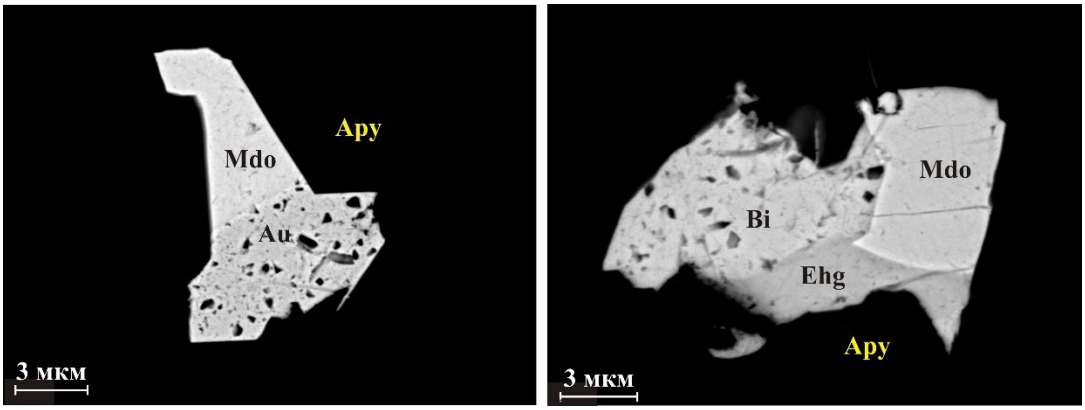

Figure 13. Maldonite with gold, native bismuth and ehrigite in polymineral inclusions in arsenopyrite-2, BSE-images. Apy – arsenopyrite, Au – native gold, Bi – native bismuth, Ehr – ehrigite, Mdo – maldonite.

Table 2. Microprobe data for ehrigite (Ehg), hedleyite (Hdl), maldonite (Mdo), and native bismuth (Bi) of the Maljavr gold occurrence, mas.%.

Mineral	Ehg	Ehg	Ehg	Ehg	Ehg	Ehg	Ehg	Hdl	Hdl	Mdo	Mdo	Bi	Bi	Bi
S	bdl	bdl	bdl	bdl	bdl	bdl	bdl	bdl	bdl	bdl	bdl	0.06	bdl	bdl
Fe	0.27	bdl	bdl	0.45	0.27	0.96	1.33	bdl	bdl	bdl	2.89	0.27	0.27	1.37
As	0.08	bdl	bdl	0.00	0.03		0.10	bdl	bdl	bdl	0.12	0.13	0.05	0.14
Te	18.61	18.68	18.34	16.38	18.29	18.36	18.25	23.45	24.93	bdl	bdl	0.00	bdl	bdl
Au	bdl	bdl	bdl	bdl	bdl	bdl	bdl	bdl	bdl	63.78	62.82	bdl	bdl	bdl
Pb	bdl	0.78	bdl	bdl	bdl	0.94	bdl	4.08	bdl	bdl	bdl	bdl	bdl	bdl

 doi:10.20944/preprints202403.1492.v1

Bi	81.49	80.54	80.23	82.49	80.36	79.64	79.05	72.47	75.07	36.22	33.85	99.02	99.88	98.43
Total	100.45	100.00	98.56	99.39	98.95	99.89	98.73	100.00	100.00	100.00	99.68	99.49	100.20	99.94
Atoms per formula unit														
S				0.047								0.004		
Fe	0.099			0.168	0.099	0.347	0.479				0.291	0.010	0.010	0.049
As	0.022				0.008		0.028				0.009	0.004	0.001	0.004
Te	2.962	3.006	2.998	2.646	2.956	2.896	2.879	3.340	3.523			0.000		
Au										1.954	1.791			
Pb		0.077				0.091		0.358						
Bi	7.917	7.915	8.003	8.140	7.934	7.667	7.615	6.302	6.477	1.046	0.910	0.982	0.989	0.947

Notes: bdl = below the detection limit. Atoms per formula unit are calculated for 11 atoms in ehrigite, 10 atoms in hedleyite, and 3 atoms in maldonite.

Table 3. Microprobe data for native gold of the Maljavr gold occurrence , mas.%.

Fe	1.94	0.48	1.48	1.12	1.71	0.77	0.24	1.11	0.11	0.24	1.35	1.67
As	0.04	0.01	0.04	bdl	0.03	0.07	0.10	0.11	bdl	bdl	bdl	bdl
Ag	7.34	21.22	35.73	45.78	3.78	4.78	29.71	8.78	18.17	18.68	6.23	bdl
Au	88.97	77.08	61.42	53.10	94.19	92.83	69.32	89.45	77.69	78.62	91.16	99.22
Total	98.29	98.80	98.67	100.00	99.71	98.46	99.37	99.45	95.98	97.53	98.75	100.89
Atoms per formula unit												
Fe	0.063	0.014	0.040	0.028	0.056	0.026	0.007	0.036	0.003	0.007	0.044	0.056
As	0.001	0.000	0.001		0.001	0.002	0.002	0.003				
Ag	0.123	0.330	0.494	0.594	0.064	0.084	0.435	0.146	0.298	0.300	0.106	
Au	0.814	0.656	0.465	0.378	0.879	0.889	0.556	0.816	0.698	0.692	0.850	0.944

3.3. Zircons in the Rocks of the Maljavr Occurrence and Age of Zircons

Zircon from sample SHM-12 of biotite gneiss-metaconglomerate forms euhedral transparent pale yellow fractured crystals, with plain facets and smoothed edges. Prism {110} and di-pyramid {111} facets are predominant. The crystal size is 50–150 μm, the elongation coefficient varies from 2.0 to 3.0. Coarse zoning was noted in the outer part of some zircon crystals. Eight samples of the least altered zircon crystals, selected from different size fractions, were assayed for U and Pb isotopes (Table 4). Analytical points of isotopic composition of eight zircon fractions lie in discordia with the age 2665±22 Ma at the upper intersection with the concordia, MSWD=9.5 (Figure 14). The lower intersection with age 380±93Ma reflects the age of Paleozoic tectonic activity and formation of the Khibiny and Lovozero alkaline intrusions [26].

Zircon from sample SHM-11 of tourmaline granite pegmatite forms euhedral long-prysmatic transparent fractured crystals of brown color. Prism {110} and di-pyramid {111} facets are predominant, the crystal faces are rough, and the edges are sharp. The inner structure is nonhomogeneous, with dark and light areas of irregular form, some grains contain inclusions of a black mineral. The crystal size is 100–300 μm, the elongation coefficient varies from 3.0 to 4.0. Five samples of the least altered and free of inclusions zircon crystals were selected from different size fractions and assayed for U and Pb isotopes (Table 4). Analytical points of isotopic composition of five zircon fractions lie in discordia with the age 2508±7 Ma at the upper intersection with the concordia, MSWD=1.4 (Figure 15). The lower intersection with the concordia occurs at 358±57 Ma.

 doi:10.20944/preprints202403.1492.v1

Table 4. Results of U–Pb geochronological studies of zircons from biotite gneiss-metaconglomerate and tourmaline granite-pegmatite.

Sample No./ Fraction No.	Weight, mg/ Size, μm	Pb, ppm	U, ppm	Isotope ratios		
				$^{206}Pb/^{204}Pb$*	$^{207}Pb/^{206}Pb$*	$^{208}Pb/^{206}Pb$*
Sample SHM-12 – biotite gneiss						
SHM-12/1	0.2/<100	165	358	533	0.1999±0.0001	0.1281±0.0002
SHM-12/2	0.5/>100	130	341	702	0.1907±0.0001	0.1246±0.0002
SHM-12/3	0.5/>100	141	337	822	0.1891±0.0001	0.1291±0.0002
SHM-12/4	0.2/>50	164	363	485	0.1972±0.0001	0.3042±0.0001
SHM-12/5	0.5/<100	361	803	1178	0.1845±0.0001	0.2709±0.0001
SHM-12/6	0.3/<50	158	371	539	0.1909±0.0001	0.2773±0.0001
SHM-12/7	0.4/<50	186	432	818	0.1829±0.0001	0.2064±0.0001
SHM-12/8	0.4/<100	175	406	1242	0.1829±0.0001	0.2062±0.0001
Sample SHM-11 - granite pegmatite						
SHM-11/1	0.3/<200	1218	2587	1426	0.1724±0.0001	0.03001±0.0001
SHM-11/2	0.9/<150	729	1534	1233	0.1741±0.0001	0.05311±0.0002
SHM-11/3	0.6/>100	793	1619	1723	0.1719±0.0001	0.02737±0.0001
SHM-11/4	1.7/>250	1109	2370	2347	0.1695±0.0001	0.02410±0.0001
SHM-11/5	1.2/>200	1140	2643	2091	0.1686±0.0001	0.02238±0.0001

Table 4. (ending).

Sample No./ Fraction No.	Weight, mg/ Size, μm	Isotope ratios		Rho	Age, Ma		
		$^{206}Pb/^{238}U$	$^{207}Pb/^{235}U$		$^{206}Pb/^{238}U$	$^{207}Pb/^{235}U$	$^{207}Pb/^{206}Pb$
Sample SHM-12 – biotite gneiss							
SHM-12/1	0.2/<100	0.3958±0.0015	9.669±0.038	0.91	2150±9	2404±10	2627±3
SHM-12/2	0.5/>100	0.3322±0.0049	7.9400±0.012	0.99	1849±27	2224±33	2590±2
SHM-12/3	0.5/>100	0.3639±0.0011	8.7448±0.026	0.96	2000±6	2312±7	2599±2
SHM-12/4	0.2/>50	0.3418±0.0014	8.1055±0.040	0.91	1896±8	2243±11	2577±4
SHM-12/5	0.5/<100	0.3551±0.0007	8.5313±0.017	0.94	1959±4	2289±5	2599±1
SHM-12/6	0.3/<50	0.3226±0.0016	7.6289±0.038	0.96	1834±9	2188±11	2539±3
SHM-12/7	0.4/<50	0.3457±0.0010	8.2387±0.025	0.88	1962±6	2258±7	2538±2
SHM-12/8	0.4/<100	0.3565±0.0011	8.5121±0.025	0.92	1966±6	2287±7	2588±2
Sample SHM-11 - granite pegmatite							
SHM-11/1	0.3/<200	0.4633±0.0005	10.509±0.011	0.90	2463±2	2481±2	2495±1
SHM-11/2	0.9/<150	0.4449±0.0007	10.068±0.015	0.95	2373±4	2441±4	2499±1
SHM-11/3	0.6/>100	0.4715±0.0011	10.714±0.026	0.99	2490±6	2499±6	2506±1
SHM-11/4	1.7/>250	0.4529±0.0009	10.265±0.021	0.96	2408±5	2459±5	2501±1
SHM-11/5	1.2/>200	0.4182±0.0009	9.3869±0.017	0.94	2252±5	2377±5	2485±1

*Isotope ratios are corrected for the blank and common lead; Rho - the correlation coefficient of the $^{207}Pb/^{235}U$-$^{206}Pb/^{238}U$ ratios.

Preprints.org (www.preprints.org) | NOT PEER-REVIEWED | Posted: 26 March 2024 doi:10.20944/preprints202403.1492.v1

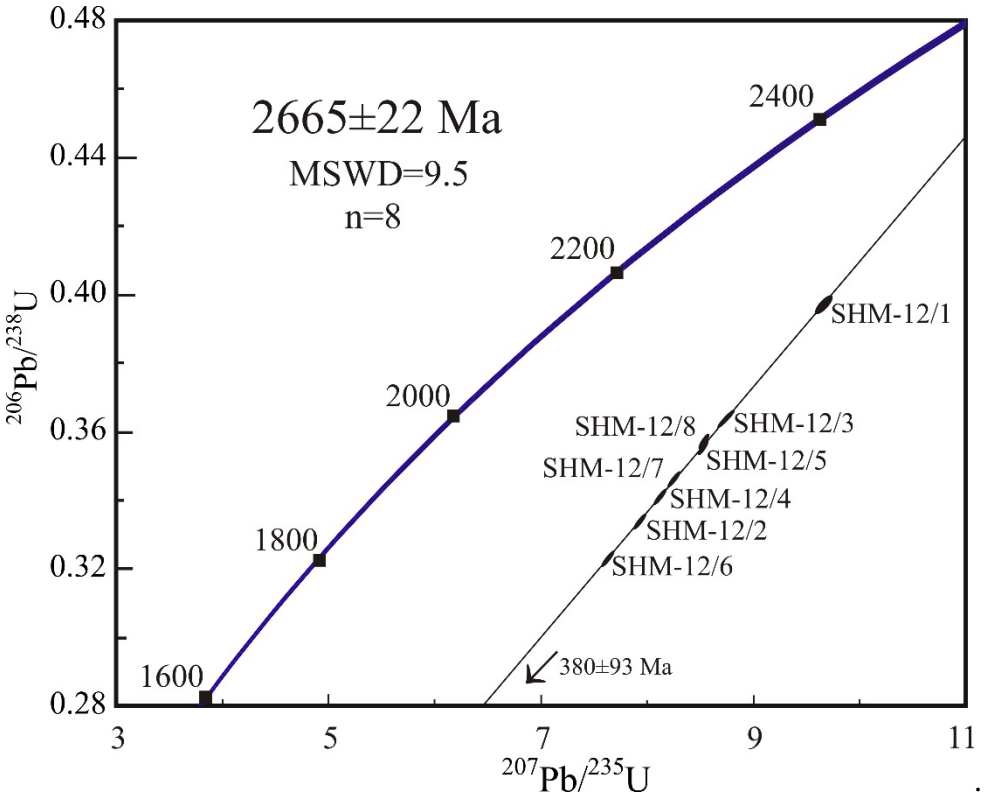

Figure 14. Diagram with concordia for the biotite gneiss from the Maljavr occurrence.

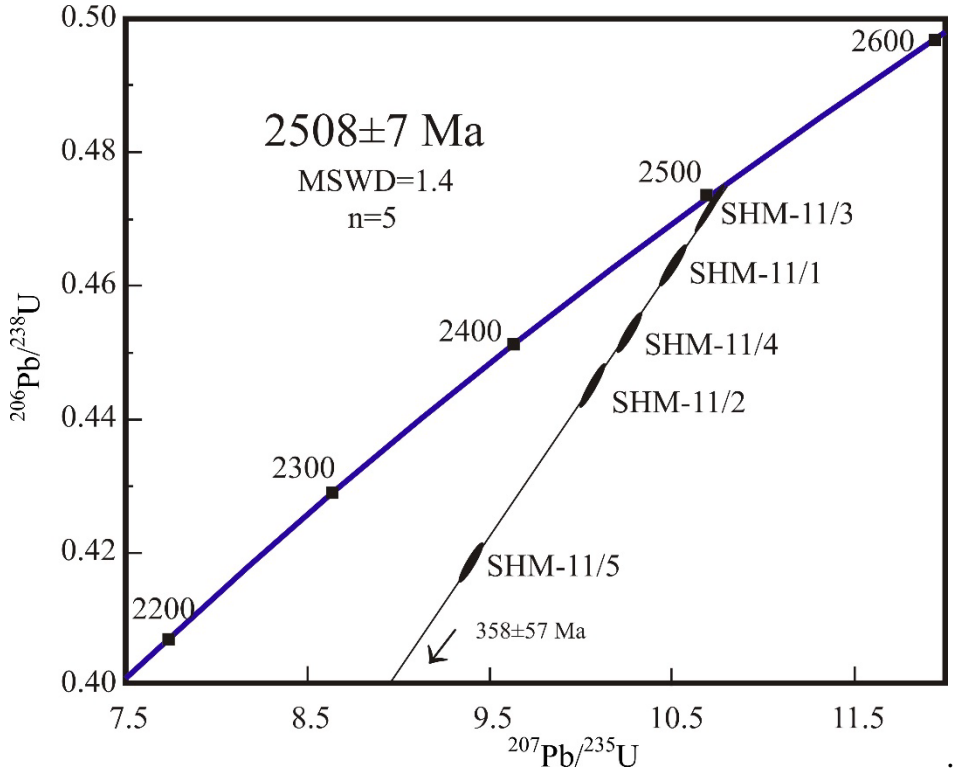

Figure 15. Diagram with concordia for the tourmaline granite pegmatite from the Maljavr occurrence.

4. Discussion

The story of formation of the Maljavr gold occurrence includes 4 stages as minimum.

 doi:10.20944/preprints202403.1492.v1

The first stage was formation of volcanic-sedimentary sequence in the Uragubsky belt, including deposition of conglomerate layers at the base and throughout the entire terrigenous sequence during the period from 2.95 to 2.83 Ga. The lower boundary of the time interval is defined by the age of detrital zircons from the basal conglomerates 2952–2939 Ma: the zircons are primary magmatic, the probable parental rock was TTG gneiss in the Kola-Norwegian block [15]. The upper boundary of the time interval of deposition of conglomerates is specified by the age gneiss-metadacite 2838 ± 23Ma (zircon, U-Pb, SHRIMP II) in the upper sequence of the belt [16]. The biotite-gneiss – metaconglomerate contains high As.

The second stage of formation of the Maljavr gold occurrence was connected with the regional metamorphism of the volcanic sedimentary sequence during the period from 2.87 to 2.66 Ga. It was the time of several accretion events, which lead to formation of the continent Kenorland [27]. An ancient island arc (the Kolmozero-Voron'ya and Uragubsky greenstone belts, at present) and the Kola-Norwegian block were successively accreted to the Murmansk block from south-west (in the modern coordinates) 2.78-2.76 Ga ago.

Volcanic-sedimentary rocks of the belt were amphibolite metamorphosed at a temperature of 600–620°C, under a pressure of 4 kbar [18]. The peak of the metamorphic event was reached at ~2.77 Ga: the U-Pb age of metamorphism is 2786 ± 31, 2774 ± 12 Ma (SHRIMP-II, zircons of metamorphic genesis) [16,17], 2763 ± 8 Ma [15].

The rocks of the Kola-Norwegian province (adjacent to the Uragubsky belt from SE) were granulite metamorphosed later, during the period 2.71–2.50 Ga. This metamorphic event was dated with the outer zones of zircon crystals, which defined the interval 2707 – 2656 Ma [28], and with zircon from biotite-garnet-sillimanite gneiss 2648 ±18 Ma [29]. Close age 2645–2675 Ga (U-Pb, SHRIMP) was obtained for the outer zones of zircon grains from skarnoids in the Olenegork iron quartzite deposit [30], it was considered as the time of alteration processes and formation of skarnoids.

The tectonic events 2.71–2.50 Ga in the Kola Norwegian block reflected in the neighboring Uragubsky and Kolmozero-Voron'ya greenstone belts. The volcanic-sedimentary sequences of the belts were intruded with plagiomicrocline granites 2696 ± 9 Ma [19]. Some zircons from the basal conglomerates in the Uragubsky belt are 2663 Ma old. Biotite-andalusite gneiss in the Kolmozero-Voron'ya belt was altered 2629±64 Ma [31].

Age of zircon from the biotite gneiss in the zone of alteration in the Maljavr occurrence is 2665±22 Ma: this age we consider as the time of alteration of the biotite gneiss, when the lenses of metasomatic rocks with sulfide (pyrrhotite-arsenopyrite) mineralization formed.

Textural and structural characteristics of the metasomatic rocks, such as massive texture with different orientation of biotite flakes and amphibole crystals, indicate alteration processes after the peak of regional metamorphism. Numerous quartz veinlets, oriented along the strike of the lenses of metasomatic rocks (Figure 5) can be accounted for hydrothermal alteration under conditions of stretching. Temperature of alteration processes was close to the temperature of the regional metamorphism: garnet-biotite geothermometer [32,33], applied to the composition of coexisting biotite and almandine in metasomatic rocks, indicates temperature 600-650°C [34].

The most recent recognized stage of formation of the Maljavr occurrence was the injection of tourmaline pegmatite veins with age of 2508±7 Ma. The pegmatite affected the biotite gneiss and metasomatic rocks and caused tourmalinization and recrystallization of sulfides: a chain of arsenopyrite grains, recrystallized due to pegmatite injection, can be seen in a thin veinlet of biotite gneiss between two lenses of pegmatite (Figure 10). Recrystallization of sulfides resulted in formation of gold-bismuth mineralization in a form of numerous inclusions in arsenopyrite-2 and löllingite grains.

Temperature of formation of arsenopyrite-2 (and gold-bismuth mineralization) was determined with arsenopyrite geothermometer [35]. The arsenopyrite geothermometer is believed to be the most reliable for sulfide systems, because arsenopyrite composition is resistant to change of PT-parameters in the surrounding medium [36]. The thermometer can be applied only to arsenopyrites with Co and Ni impurities less than 0.5 mas.%: arsenopyrite-1 does not fit this demand, but arsenopyrite-2 is

 doi:10.20944/preprints202403.1492.v1

acceptable (Table 1). Composition of arsenopyrite-2 and its association with pyrrhotite indicate two temperature intervals: 500 – 600°C for arsenopyrite with As 34,6-35,9 at% and 400 – 510°C for arsenopyrite with As 32,7 – 33,8 at%. The first interval can be related to the temperature of metamorphism, and the second corresponds well to the temperature of pegmatite crystallization T = 415–460 °C, estimated with different mineral thermometers and study of fluid inclusions in beryl from the area of the Maljavr occurrence [37].

Visible gold was found exceptionally in arsenopyrite-2 and löllingite, which were recrystallized at the time of pegmatite injection; therefore pegmatite age 2508±7 Ma reflects the time of formation of gold-bismuth mineralization.

Geological position of the Maljavr occurrence, geochemical association Au-As-Se-Te-Bi in the mineralized rocks, and the linkage of gold mineralization with pegmatite – all these characteristics correspond well to the type of reduced intrusion related gold deposits [38–40]. Biotite gneiss-metaconglomerate, hosting the mineralized metasomatic rocks, could be the primary source of arsenic and, probably, gold for mineralization, which formed later.

5. Conclusions

The following story of formation of the Maljavr gold occurrence is reconstructed:

1. Deposition of sedimentary rocks, including conglomerates with high As and, probably, gold, in the interval 2.95 – 2.83 Ga
2. Regional upper amphibolite metamorphism of volcanic-sedimentary sequence in the interval 2.77 – 2.79 Ga.
3. Alteration of biotite gneiss-metaconglomerate and formation of lenses of metasomatic rocks with sulfide pyrrhotite-arsenopyrite mineralization; this event took place in a local zone of NNE strike at ~2.66-2.67 Ga. Geochemical association of the altered rocks includes As, Ag, Se, Te, Bi, and Cu.
4. Injection of tourmaline pegmatite veins at ~2.51Ga caused recrystallization of sulfides and formation of gold-bismuth mineralization. Gold and bismuth minerals (native gold, maldonite, native bismuth, ehrigite and other tellurides) occur exceptionally in inclusions in recrystallized arsenopyrite (arsenopyrite-2) and löllingite.

Biotite gneiss-metaconglomerate, hosting the mineralized metasomatic rocks, was the probable primary source of arsenic and gold for mineralization, which formed later. Geological position of the Maljavr occurrence, the linkage of gold mineralization with pegmatite, geochemical association Au-As-Se-Te-Bi in the mineralized rocks correspond to the type of gold deposits, associated with intrusions.

The Maljavr occurrence in the first gold occurrence in the Fennoscandian Shield, located in Archean conglomerates.

Supplementary Materials: The following supporting information can be downloaded at the website of this paper posted on Preprints.org. Table S1: Chemical composition of biotite gneiss-metaconglomerate and altered rocks; Table S2: Microprobe data for rock-forming minerals, Table S3: Content of minor elements in biotite gneiss-metaconglomerate and altered rocks.

Author Contributions: Conceptualization, A.K. and N.K.; methodology, A.K.; investigation, A.K., N.K. and Ye.S.; writing—original draft preparation, A.K. and N.K.; writing—review and editing, A.K., N.K. and Ye.S; project administration, N.K.; funding acquisition, N.K. All authors have read and agreed to the published version of the manuscript.

Funding: The work was carried out under Project FMEZ-2024-0004 of the Russian Academy of Science.

Data Availability Statement: The data presented in this study are available on request from the corresponding author.

Acknowledgments: The authors thank students of the Murmansk State Technical University Alexandr Ermolin, Mariam Khachatryan, Elena Galeeva, and Julia Samsonova for productive work in the field, Tatiana Zykova and Elena Galeeva for preparation of the samples for microprobe analyses.

Conflicts of Interest: The authors declare no conflicts of interest.

 doi:10.20944/preprints202403.1492.v1

References

1. Tucker, R.F.; Viljoen, R.P.; Viljoen, M.J. A review of the Witwatersrand Basin. *Episodes* **2016**, 39, 105–134.
2. Smith, A.J.B.; Henry, G.; Frost-Killian, S. A review of the Birimian Supergroup- and Taerwaian Group-hosted gold deposits of Ghana. *Episodes* **2016**, 39, 177–198.
3. Milesi, J.P.; Ledru, P.; Marcoux, E.; Mougeot, R.; Johan, V.; Lerouge, C.; Sabate, P.; Bailly, L.; Respaut, J.P.; Skipwith, P. The Jacobina Paleoproterozoic gold-bearing conglomerates, Bahia, Brazil: a "hydrothermal shear-reservoir" model. *Ore Geol. Rev*. **2002**, 19, 95–136.
4. Munroe, S.; Cunningham, M.. The Pilbara's Conglomerate Gold. *Australian Resources and Investment* **2018**, 12, 74–76.
5. Chakravarti, R.; Singh, S.; Akella, V.S. Gold Mineralisation within Quartz Pebble Conglomerates of Gorumahisani Badampahar Schist belt, Singhbhum Craton, Eastern India. *J Geosciences Research* **2017**, 1, 27–34.
6. Ulrich, T.; Long, D.G.F.; Kamber, B.S.; Whitehouse, M. In-situ trace element and sulfur isotope analysis of pyrite in a Paleoproterozoic gold placer deposit, Pardo and Clement Townships, Ontario, Canada. *Econ. Geol*. **2011**, 106, 667–686.
7. Long, D.G.F.; Ulrich, T.; Kamber, B.S. Laterally extensive modified placer gold deposits in the Paleoproterozoic Mississagi Formation, Clement and Pardo Townships, Ontario. *Canadian Journal of Earth Sciences* **2011**, 48, 779–792.
8. Website of the Department of Use of Underground and Ecology of the Karelian Republic. http://nedrark.karelia.ru/mnia/au_karelia.htm. Electronic Resource, accessed 10.12.2023.
9. Krogh, T.E. A low-contamination method for hydrothermal decomposition of zircon and extraction of U and Pb for isotopic age determination. *Geochim. Cosmochim. Acta* **1973**, 37, 485–494.
10. Ludwig, K.R. PbDat for MS-DOS, Version 1.21; *U.S. Geological Survey Open-File Report*; U.S. Geological Survey: Reston, VA, USA, 1991; pp. 88–542.
11. Ludwig, K.R. ISOPLOT/Ex. Version 2.06. *A Geochronological Toolkit for Microsoft Excel*; Berkley Geochronology Center Special Publication: Berkeley, CA, USA, 1999, 49 p.
12. Steiger, R.H.; Jager, E. Subcomission of geochronology: Convention of the use of decay constants in geo- and cosmochronology. *Earth Planet. Sci. Lett*. **1976**, 36, 359–362.
13. Stacey, J.S.; Kramers, I.D. Approximation of terrestrial lead isotope evolution by a two-stage model. *Earth Planet. Sci. Lett*. **1975**, 26, 207–221.
14. Smol'kin, V. F.; Mezhelovskaya, S. V.; Mezhelovsky, A. D. The Sources of the Clastic Material of the Terrigenous Sequences of the Neoarchean and Paleoproterozoic Paleobasins in the Eastern Part of the Fennoscandian Shield Based on Isotope Analysis Data for Detrital Zircons (SIMS, LA-ICP-MS). *Stratigraphy and Geological Correlation* **2020**, 571–602.
15. Myskova, T.A.; Mil'kevich, R.I.; Bogomolov, Ye.S.; Guseva, V.F. New data on composition and age of the protolith of the high-alumina gneisses of the Kolskaya and Tundrovaya series. Geology and Geodynamics of the Archean: *Proceedings of the I Russian Conference on the problems in geology and geodynamics of the Precambrian*. Sankt-Peterburg 2005, IGGP, 272–275. (In Russian)
16. Myskova T.A.; Glebovitsky, V.A.; Mil'kevich, R.I.; Berezhnaya, N.G.; Skublov, S.G. Improvement of composition and age of aluminum gneisses of the Uragubskaya greenstone Later Achaean structure, Kola Peninsula, *Proc. Russ. Min. Soc.* **2010**, 139, 3, 15–21. (In Russian)
17. *The Early Precambrian of the Baltic Shield*. Glebovitsky, V.A. (ed.) Sankt-Peterburg, Russia, Nauka, 2005, 711 p. (In Russian)
18. Vrevskii, A.B. Specifics of Neoarchean plume–lithospheric processes in the Kola–Norwegian Province of the Fennoscandian Shield: I. Composition and age of the komatiite–tholeiite association, *Petrology* **2018**, 26, 121–144.
19. Bogdanova, V.S.; Dagelayskiy V.B. Age position of the rocks of the Tundrovaya series and conglomerates in the area of Ura river (Kola Peninsula). *Absolute age of the Precambrian rocks in the USSR*. Moscow-Leningrad, Russia, Nauka, 1965, 74–83. (In Russian)
20. Smolkin, V.F.; Borisova, V.V., Svetov, S.A., and Borisov, A.E. Late Archean komatiites of the Ura Bay–Titovka Structure, northwestern Kola region. *Petrology* **2000**, 8, 177–199.
21. Voronyaeva, L.V.; Krupenik, Z.V. A new gold prospect in the Titovsko-Uragubskaya greenstone Late Archean structure (Kola region). *Regional geology and metallogeny* **2021**, 86, 82–91. DOI: 10.52349/0869-7892_2021_86_82-91. (In Russian)
22. Stanley, C. Molar Element Ratio Analysis of Lithogeochemical Data: A Toolbox for Use in Mineral Exploration and Mining. *Proceedings of Exploration 17: Sixth Decennial International Conference on Mineral Exploration*, Tschirhart, V. and Thomas, M.D. (ed.), 2017, 471–494.
23. Warr L.N. IMA–CNMNC approved mineral symbols. *Mineralogical Magazine* **2021**, 85. 291–320. https://doi.org/10.1180/mgm.2021.43
24. Taylor, S.R.; McLennan, S.M. *The Continental Crust: Its Composition and Evolution*. Blackwell, Oxford, 1985, 312 p.

25. Kramm, U.;, Kogarko, L.N.; Kononova, V.A.; Vartiainen, H. The Kola alkaline province of the CIS and Finland: Precise Rb-Sr ages define 380-360 age range for all magmatism. *Lithos* **1993**, 30, 33-44.
26. Ciobanu, C. L.; Cook, N. J.; Yao, J.; Slattery, A.; and Wade, B. Ehrigite, IMA 2023-074, in: CNMNC Newsletter 77, *Eur. J. Mineral*. **2024**, 36, 165-172. https://doi.org/10.5194/ejm-36-165-2024.
27. Mints, M.V.; Suleimanov, A.K.; Babayants, P.S. *Deep Structure, Evolution, and Minerals in the Early Precabrian Basement of the East European Platform: Interpretation of Materials on Referent Profile 1-EV, Profiles 4V and TATSEIS*; Geokart Geos: Moscow, Russia, 2010; ISBN 978-5-89118-531-9. (In Russian)
28. Balashov Yu. A., Mitrofanov F. P., Balagansky V. V. New geochronological data on Archaean rocks of the Kola Peninsula. *Correlation of Precambrian formations of the Kola-Karelian region and Finland*. Apatity: Kola Science Centre of the Russian Academy of Sciences. 1992, 13–34. (In Russian)
29. Myskova, T.A., Milkevich, R.I. Aluminiferous gneisses of the Kola series, Baltic Shield (geochemistry, nature and age of protolith), *Tr. Karel. Nauchn. Tsentra RAN* **2016**, 10, 34–62. (In Russian)
30. Goryainov, P.M.; Ivanyuk, G.Y.; Bayanova, T.B.; Bazay, A.V.; Astaf'ev, B.Y.; Voinova, O.A. Composition, genesis, and age of rare-earth and precious metal mineralization in the rocks of banded iron formation in the Kola Peninsula. *Proc. Fersman Sci. Sess*. **2012**, 9, 235–238. (In Russian)
31. *State geological map of Russian Federation. Scale 1:1000000 (the third generation). Series Severo-Karsko-Barentsevomorskaya. Sheet R- 37, 38 – cape Svyatoy Nos, cape Kanin Nos. Explanatory note*. Sankt-Peterburg: Kartograficheskaya fabrika VSEGEI, 2008, 251 p. (in Russian)
32. *Thermo- and barometry of metamorphic rocks*. Glebovitsky, V. A. (ed.). Leningrad, Russia, 1977, 207 p. (In Russian)
33. Gul'bin, Yu.L. Optimization of the garnet-biotite geothermometer. 1. Temperature trends. *Proc. of the Russian Min. Soc.* **2010,** 139, 5, 1–17. (In Russian)
34. Kalinin, A. A.; Kudryashov, N.M.; Savchenko, Ye.E. Mal'javr – the first gold prospect in the Archean conglomerates, the Kola region. *Vestnik of MSTU* **2023**, 26, 5–17. (In Russian). DOI: https://doi.org/10.21443/1560-9278-2023-26-1-5-17.
35. Kretschmar, U., Scott, P.D. Phase relations involving arsenopyrite in the system Fe-As-S and their application. *Canadian Mineralogist* **1976**, 14, 363–386.
36. Tyukova, Ye. E.; Voroshin, S. V. *Arsenopyrite mineral composition and parageneses in ore deposits and host rocks throughout the Upper Kolyma River area (interpreting the genesis of sulfide mineral assemblages)*. Magadan, Russia, 2007, 108 p. (In Russian)
37. Ponomareva, N.I.; Gordienko, V.V.; Shurekova, N.S. Physicochemical circumstances of beryl generation in "Bol'shoy Lapot" deposit (Kola Peninsula). *Vestnik of Sankt-Peterburg University, series 7* **2015**, 3, 4-20. (In Russian)
38. Groves, D.I.; Santosh, M. Province-scale commonalities of some world-class gold deposits: Implications for mineral exploration. *Geoscience Frontiers* **2015**, 6, 389-399 DOI: 10.1016/j.gsf.2014.12.007
39. Hart C.J.R. Reduced intrusion-related gold systems. *Mineral deposits of Canada: A Synthesis of Major Deposit Types, District Metallogeny, the Evolution of Geological Provinces, and Exploration Methods*. Geological Association of Canada, Mineral Deposits Division, Special Publication No. 5, 2007, 95-112.
40. Baker, T.; Lang, J.R. Fluid inclusion characteristics of intrusion related gold mineralization, Tombstone-Tungsten magmatic belt, Yukon Territory, Canada. *Mineral. Depos*. **2001**, 36, 563—582.